Chapter 3

Numerical and Experimental Study on Constrained Groove Pressing

Yanjin Guan and Zongshen Wang

Additional information is available at the end of the chapter

http://dx.doi.org/10.5772/intechopen.68504

Abstract

Constrained groove pressing (CGP) is a new severe plastic deformation method suitable for producing ultra-fine grained sheet metals. Based on Taguchi optimization method, the influence of processing parameters such as groove width, groove angle, friction coefficient and deformation rate on deformation homogeneity of constrained groove pressing (CGP) was studied numerically utilizing DEFORM-3D. A multi-pass CGP was carried out on 1060 commercially pure aluminium, copper and Ni sheets. Through a series of experimental research, the evolution of microstructure, tensile properties, forming load, and die parameters during the process was investigated.

Keywords: constrained groove pressing, material properties, processing efficiency, strain homogeneity, die parameters

1. Introduction

Constrained groove pressing (CGP) is one of the most attractive SPD techniques available for fabricating ultra-fine grained (UFG) sheet or plane metallic materials. Since originally proposed by Shin et al. in 2002 [1], CGP has been successfully used for grain refinement and mechanical property improvement of various sheet metals and alloys. In this technique, the sheet sample is subjected to repetitive shear deformation via alternant pressings by asymmetrically groove dies and flat dies. Thus, a large strain can be uniformly accumulated throughout the whole sample without any significant change in its dimensions. As a result, a relatively homogeneous UFG structure can be obtained.

A schematic illustration of CGP process is shown in **Figure 1**. Before pressing, a set of asymmetrical groove dies (**Figure 1a**) and a set of flat dies (**Figure 1c**) are prepared. At first, the sample is pressed into the groove dies with a groove width, T, and a groove angle θ (**Figure 1a**). The gap

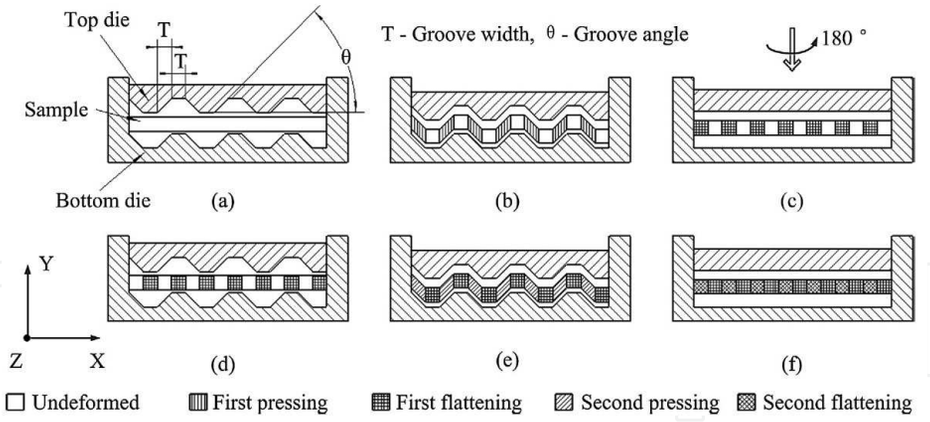

Figure 1. Schematic of constrained groove pressing (CGP).

between top and bottom dies is kept the same with the sample thickness. Thus, the inclined regions of the sample are subjected to pure shear deformation under plane strain condition while no deformation is induced in the flat regions (**Figure 1b**). Then, the grooved sample is placed between the flat dies and straightened (**Figure 1c**). Due to the tight constraint from the side walls of bottom die, the inclined regions previously deformed experience reverse shear deformation while the flat regions remain undeformed. After that, a rotation of the sample by 180° about Y-axis which is perpendicular to the sheet plane is performed (**Figure 1d**). This ensures the undeformed regions to be deformed during the second groove pressing (**Figure 1e**) and flattening (**Figure 1f**) due to the asymmetry of the groove dies. Thus, the alternate pressings with groove dies and flat dies result in a homogenous strain distribution throughout the sample without any changes in its dimensions. Generally, two groove pressings and two flattenings compose one CGP pass. Finally, a relatively uniform UFG structure can be obtained after a multi-pass CGP.

The theoretical equations for calculating the shear and effective strains accumulated for one pressing can be derived from **Figure 1**. A single pressing induces an engineering shear strain,

$$\gamma_{xy} = \tan\theta \tag{1}$$

where H, T, and θ are groove height, width, and angle, respectively. Shear strain is given as

$$\varepsilon_{xy} = \gamma_{xy}/2 \tag{2}$$

Since CGP is assumed as a pure shear deformation under plane strain condition [2], correspondingly, the effective strain,

$$\varepsilon_{eff} = \sqrt{\frac{4\varepsilon_{xy}^2}{3}} = \sqrt{\frac{4(\gamma_{xy}/2)^2}{3}} = \frac{\gamma_{xy}}{\sqrt{3}} = \frac{\tan\theta}{\sqrt{3}} \tag{3}$$

Therefore, the total effective strain accumulated in a CGP sample pressed by n passes is presented as

$$\varepsilon_{total} = n\frac{2\tan\theta}{\sqrt{3}} \tag{4}$$

Specifically, when the groove angle, θ is 45°, the groove width, T is equal to the groove height, H. Then, the engineering shear strain, $\gamma_{xy} = 1$, and the effective strain, $\varepsilon_{eff} = 1/\sqrt{3} \approx 0.58$. In this case, theoretically, one CGP pass induces a total effective strain of about 1.16 in the sample. Obviously, the groove angle, θ, directly determines the efficiency of strain accumulation.

CGP exhibits a great potential in producing UFG sheet metals, and until now, it has been successfully used for grain refinement and mechanical property improvement of various pure metals and alloys. From the process, significant influences on CGP by the structural parameters of groove dies including groove angle and width are expected. However, very limited studies are focused on this topic, and researchers still cannot reach an agreement on the influence rule. For instance, Borhani and Djavanroodi [3] investigated the effects of die design on a modified CGP process called rubber pad-CGP experimentally and numerically. They found that, compared with 45°, a higher groove angle of 50°could enhance the grain refinement and mechanical property improvement but reduce the strain homogeneity. Nevertheless, in another work on a covered sheet casing-CGP carried out by Sajadi et al. [4], it was demonstrated that an increase of groove angle from 45 to 53°could not promote more CGP passes and the improvement of mechanical properties. Peng et al. [5, 6]. analyzed the effects of groove width on CGP of a Cu-Zn alloy. They found that groove dies with the width increasing from 5 to 7 mm permitted more passes without crack formation but induced a lower rate of grain refinement and a slower increase in hardness.

As can be seen, the higher pass number resulted from a larger groove width is well explained by the above discussion, but the lower process efficiency still needs more detailed analysis. Thus, based on numerical and experimental methods, a multi-pass CGP was carried out on 1060 commercially pure aluminium, copper and Ni sheets in order to study the evolution of microstructure, tensile properties, forming load, die parameters and deformation mode during the process.

2. Finite element analysis and deformation homogeneity optimization of constrained groove pressing

2.1. FE-simulation and optimization

The FE-simulation model for CGP was built up using DEFORM-3D software. The initial dimensions of the sample are 100 × 100 × 2 mm^3, and the material is aluminium alloy 5052. Both top die and bottom die are defined as a rigid body while the sample is plastic. During the deformation procedure, the bottom die is fixed and the top die moves in the $-Y$ direction at a constant speed. The coefficient of friction between the die surface and the sample is within a range (0.08–0.12) in cold forming of metals. The isothermal process is conducted at room temperature (20°C). The tetrahedral element is used for meshing and automatic re-meshing is activated. The total number of elements is 175,000 and the incremental step length is 0.2 mm. To ensure the accuracy, volume loss during simulation is taken into account. When the volume

loss exceeds 5%, corresponding volume compensation is considered. The properties of the selected material are described by the following model equation of power law form:

$$\overline{\sigma} = c\overline{\varepsilon}^{n}\,\dot{\overline{\varepsilon}}^{m} + y \tag{5}$$

where $\overline{\sigma}$ is flow stress, $\overline{\varepsilon}$ is an effective plastic strain, $\dot{\overline{\varepsilon}}$ is effective strain rate, c is material constant, n is strain exponent, m is strain rate exponent, and y is initial yield stress value. For aluminium alloy 5052, fitted values of the parameters achieved from the software are $c = 56.4MPa$, $n = 0.0396$, $m = 0.0105$ and $y = 140MPa$.

In this study, one pressing cycle includes two groove pressings and two flattenings. The data of analysis points are extracted and analyzed after the sample is deformed after four cycles. In order to reduce the error, 5 mm from both edges of the sample along the longitudinal direction is ignored. The equivalent strain values of 300 points are measured uniformly as FE-simulation results along different paths within the range of 90 mm. The illustration of the analysis point selection is shown in **Figure 2**. The central line of the cross section at $Z = 0$ is identified as Path A, and the upper edge as Path B. The central line of the cross section at $Z = 50$ is defined as Path C. Among the paths concerned above, obviously, Path A is basically the most representative one for the deformation characteristics of the whole sample.

To describe the deformation homogeneity, I.F. is adopted as the index, which can be calculated by the following expression:

$$I.F. = \frac{\sqrt{\sum_{i=1}^{i=n}(H_i - \bar{H})^2/(n-1)}}{\bar{H}} \tag{6}$$

where n is the number of analysis points, H_i is the equivalent strain value of i-th point, $\overline{H}$ is the average strain value of all the analysis points. Normally, the lower I.F. value indicates more homogeneous deformation.

Four processing parameters were analyzed synthetically. They are groove width, groove angle, friction coefficient and deformation rate. The levels of each parameter are determined and

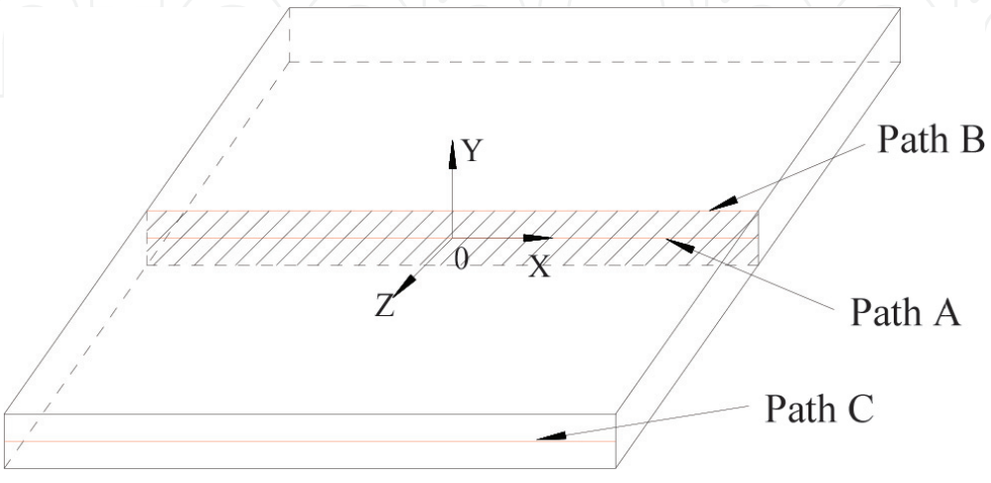

Figure 2. Extraction paths of analysis points.

shown in **Table 1**. The factors are expressed by A, B, C and D, and the levels by 1, 2 and 3. Due to the number of factors and levels chosen above, the L9 (3^4) orthogonal array is employed.

2.2. Results and discussion

The simulations of CGP for nine sets of parameter combination were conducted making use of DEFORM-3D, and values of equivalent strain for each plan were extracted along Paths A, B, and C of the deformed sample, respectively. After the I.F. value of each trial is figured out according to Eq. (6).

To examine the effect rule of the selected parameters, the mean S/N ratio for different levels of each factor are calculated, and the results are listed in **Table 2**. Since the smaller the better

Factors	Level 1	Level 2	Level 3
Groove width, A (mm)	1	1.5	2
Groove angle, B (°)	30	45	60
Friction coefficient, C	0.08	0.1	0.12
Deformation rate, D (mm/s)	0.16	1.6	16

Table 1. Analysis factors and levels.

Levels	Path A			
	A	**B**	**C**	**D**
1	26.293	24.317	28.805	28.433
2	31.176	30.882	30.094	31.005
3	31.592	33.861	30.162	29.623
Levels	**Path B**			
	A	**B**	**C**	**D**
1	26.417	24.114	27.441	28.606
2	30.742	29.838	30.120	30.200
3	30.247	33.453	29.845	28.599
Levels	**Path C**			
	A	**B**	**C**	**D**
1	26.172	18.841	25.315	25.289
2	26.832	28.505	28.598	26.685
3	26.834	32.491	25.925	27.864

Table 2. The mean *S/N* ratio for different levels of each factor.

quality characteristic was selected previously, higher value of S/N ratio implies a lower value of I.F. under the corresponding condition. Meanwhile, the CGP deformation effects are much better. Obviously, the I.F. value becomes lower as groove width, groove angle and friction coefficient increase except for deformation rate. Consequently, the best parameter combination is achieved and the combination is A3B3C3D2. When groove width is 2 mm, groove angle is 60°, the friction coefficient is 0.12 and deformation rate is 1.6 mm/s, the deformation is the most homogeneous.

The optimum result was compared with that of the initial model by applying the new parameter combination to the FE-simulation. During the initial process, the groove width is 2 mm, groove angle is 45°, the friction coefficient is 0.12 and deformation rate is 16 mm/s. It is evident that the mean amount of accumulative strain after optimization in the sample pressed by the same number of cycles is almost twice compared to the initial model. The effectiveness for grain refinement was significantly improved. Meanwhile, the difference between maximum and minimum values of equivalent strain almost keeps invariable before and after optimization. Regardless of the location of data points, the drop ranges of I.F. of equivalent strain are all about 50%, which means that the deformation homogeneity was enhanced distinctly after optimization. Furthermore, the I.F. value decreased from 0.028749 to 0.016103 and the S/N ratio rose from 30.828 to 35.866. As a result, the deformation turned to be more homogeneous.

3. Experimental investigation of pure aluminum sheets processed by constrained groove pressing

3.1. Experimental procedure

Cold-rolled 1060 commercially pure aluminum sheets with dimensions of $100 \times 100 \times 2$ mm^3 were used. Before deformation, the sheets were annealed at 500°C for 4 h in an SX2-4-10 resistance-heated furnace utilizing high pure nitrogen as the protective atmosphere to ensure the annealing process.

In experiments, molybdenum disulfide (MoS_2) was coated on the surface of sheets as a lubricant. CGP process was conducted on a 5000 kN computer-controlled electro-hydraulic servo compression testing machine operated at a constant pressing speed of 5 mm·min-1 at room temperature. The pressing dies equipped with guide pillars and bushes had a groove angle of 45° and a groove width of 2 mm. Therefore, one CGP pass contained two groove pressings and two flattenings, yielding an effective strain of 1.16 throughout the whole sheet.

3.2. Results and discussion

A four-pass CGP with a total strain of 4.64 was successfully conducted on pure aluminum sheets. The microstructure evolution is shown in **Figure 3**. The grain size was measured based on OM observation and recorded in **Table 3**. The as-received material mainly consists of uniform and equiaxed grains with an average size of 29 μm (**Figure 3a**). Also, dislocation cells sized about 1 μm or more are evident in **Figure 3b**. Submicron and dislocation-free subgrains with well-defined boundaries begin to form at Pass 3 (**Figure 3c**). In **Figure 3d**, the subgrain

http://dx.doi.org/10.5772/intechopen.68504

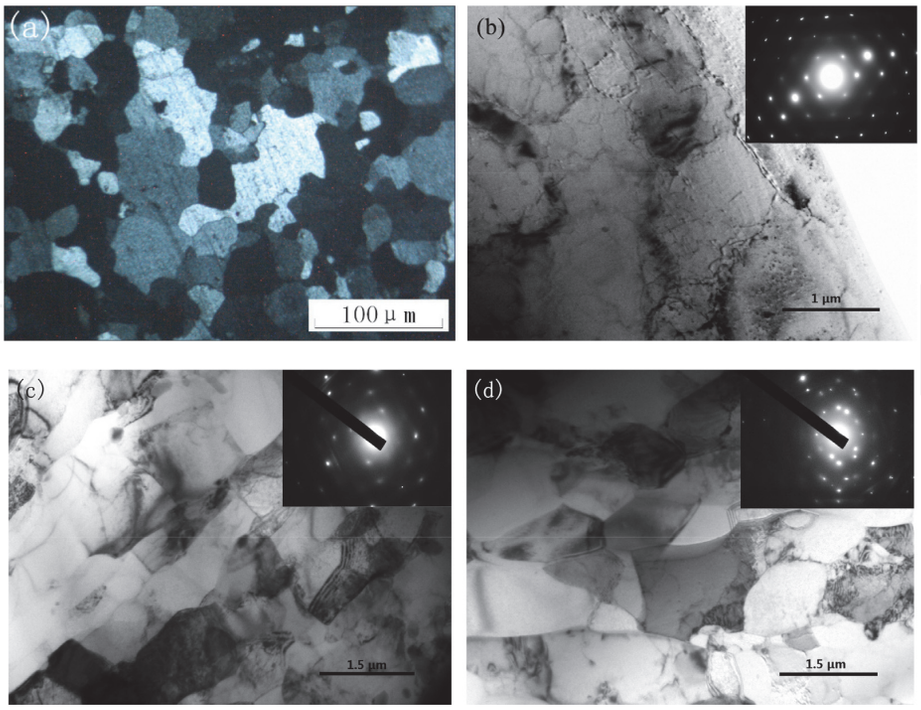

Figure 3. Optical micrograph for annealed sample (a) and TEM micrographs with their SAED patterns for (b) annealed, (c) three-pass and (d) four-pass samples, respectively.

Pass	0	1	2	3	4
Grain size (μm)	29.0	23.0	20.2	19.3	18.3
Yield strength (MPa)	23.8	93.8	98.2	103.6	93.5
Ultimate tensile strength (MPa)	66.9	101.1	109.1	111.5	96.4
Elongation to failure (%)	53.6	7.4	7.5	7.3	4.5

Table 3. Variations of grain size and tensile properties with pass number.

size undergoes a slight increase, and new tiny "grains" begin to appear along the boundaries. More diffused SAED pattern indicates higher misorientation angle between adjacent subgrains. Finally, the grain size estimated from OM observation is refined to 18 μm after Pass 4 and just 62% as that of the annealed material, as presented in **Table 3**.

Table 3 also lists the variations of tensile properties of aluminum samples with pass number. The ultimate tensile strength and yield strength increase rapidly to 101.1 and 93.8 MPa after Pass 1, respectively. However, in the following passes, they increase slowly. After that, the ultimate tensile strength and yield strength reach their maximum values, followed by reductions at Pass 4. This can be explained by the dynamic recovery of dislocations and subgrain coarsening shown in **Figure 3d**. Micro-cracks appeared on the sample surface during the later stages also contribute to the strength loss. The elongation decreases greatly from 53.6 to 7.4%. After that, it experiences a continuous and moderate reduction. No recovery of the elongation

occurs due to flow softening, indicating that the effect of micro-cracks on tensile properties of material processed by CGP is more significant than flow softening [7].

For clarity, load-stroke curves of forming dies for Passes 1 and 2 are displayed in **Figure 4a** and **b**, respectively. Obviously, forming loads for all pressings can be divided into three distinct stages: rapid increase, moderate increase and second rapid increase. At the beginning of groove pressing, groove edges firstly contact and bend the sheet. After a short elastic deformation, the material begins to yield and comes to initial shearing around the groove edges, leading to the rapid increase of forming load. Then, as the upper die moves downwards, plastic deformation extends to other areas and results in the gradual increase of flow stress. Obviously, this stage covers more than one-half of the total pressing time and is the main stage of the three. A relatively steady load can be observed at this stage. At last, the grooves contact the entire surface of the sheet. The sheet is forced to be the same shape as the groove dies. Thus, another noticeable increase of forming load appears after the dies are fully closed. The load for flattening exhibits a similar variation tendency. Interestingly, a short plateau at the initial part of the second stage is observed from each flattening curve, as presented in the red circles in **Figure 4**. This is substantially attributed to the constraint by the container of flat dies. Before the extension of the plastic deformation to other areas, the sheet extends along the longitudinal direction firstly and is fully constrained by the side walls of the container.

In addition, as illustrated in **Figure 4a**, the stage division of load-stroke curves for the first groove pressing and flattening is not as clear as that for the other pressings because no strengthening was induced to the annealed aluminum sheets. It is concluded from the curves for all passes, not shown here, that the steady forming load in the second stage increases with CGP pass and a higher increasing rate is observed during the former passes. Within one pass, the steady loads for the two groove pressings are lower than those for the two flattenings which are almost equal to those for the groove pressings of the next pass. There are several contributing factors: (a) the strengthening of material increases with pass number and saturates at a high strain magnitude, (b) the inclined regions to be deformed in flattening have already been strengthened by shear deformation from the last groove pressing, and (c) the constraint by the side walls plays a more significant role in flattening than in groove pressing.

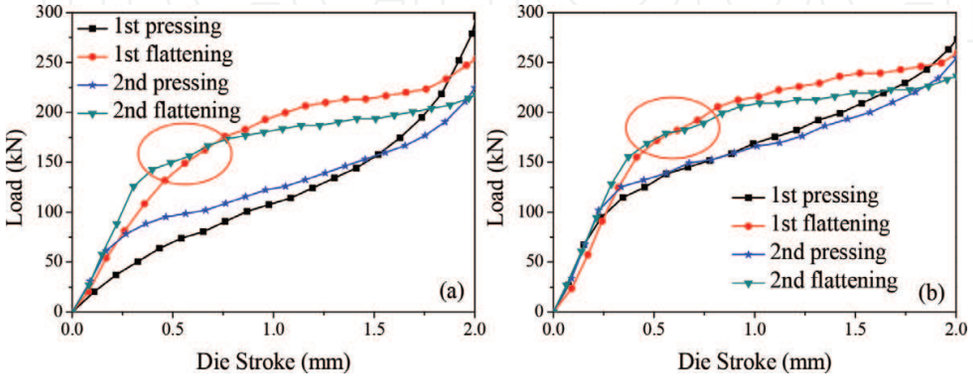

Figure 4. Load-stroke curves for (a) Pass 1 and (b) Pass 2, respectively.

4. Deformation efficiency and electrical resistivity of pure copper processed by constrained groove pressing

4.1. Experimental procedure

In the experiment, T2 commercially pure copper sheets were used. Before pressing, the sheets were annealed at 650°C for 2 h in an SX2-4-10 resistance-heated furnace with high pure nitrogen to avoid oxidation. The annealed sheets were machined to the dimensions of 100 mm × 100 mm × 2 mm. In this study, the samples underwent a four-pass CGP with a theoretically total strain of 4.64 until obvious cracks appeared on the surface of pressed samples at the last pass. The rest experimental conditions are the same with Section 3.1.

Resistances of sheets before and after CGP were measured using a four-electrode method by an H2ERM-1 resistance measuring device. A stable constant current of 500 mA provided by a PF66M digital multimeter passed through the specimen for approximately 4 s period to reduce Joule heating.

4.2. Processing efficiency

In this work, distinct cracks appear on the sheet surface at Pass 4, leading to uncompleted tensile tests. Thus, yield strength, ultimate tensile strength, and elongation to failure of materials for up to three passes are listed in **Table 4**. Great enhancement and rapid saturation of strengths are almost achieved after two passes, and further deformation induces significant decrease. Generally, this strengthening is introduced by work hardening and grain refinement. Previous papers proposed flow softening and microcracking as softening mechanisms [8–10].

Figure 5a and **b** illustrates the microstructures of pressed copper after one and three passes, respectively. In another experimental work on CGP of pure copper, only cell block structures with size of approximately 0.5 μm were obtained with a total strain of 3.48, even at cryogenic temperatures. In this study, as shown in **Figure 5a**, cell blocks with irregular shape exist as main structural features at the initial stages of straining. However, after three passes, subgrains with relatively distinct boundaries tend to be predominant in the structure, as indicated by the diffused SAED pattern in **Figure 5b**. The substructures are elongated and segmented into smaller ones, and the dislocation density inside is lower than before although the mean size remains the same. This seems to contribute to the flow softening mechanism concerned above. Meanwhile, **Table 4** also shows that the elongation decreases continuously as strain increases, and the highest rate of decrease is observed at Pass 1. No recovery of elongation happens during the last stages. Thus, it suggests that, during the whole CGP process, the drop of

Pass	0	1	2	3	4
Yield strength (MPa)	43.8	303.1	304.3	162.1	—
Ultimate tensile strength (MPa)	209.5	313.6	323.7	191.0	—
Elongation to failure (%)	51.5	6.1	5.7	3.0	—

Table 4. Tensile properties of pure copper samples.

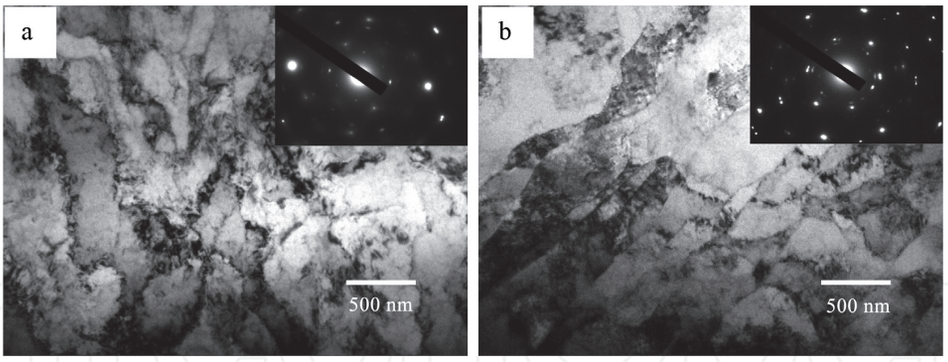

Figure 5. TEM micrographs and corresponding SAED patterns of copper after: (a) one and (b) three passes, respectively.

elongation caused by work hardening and microcracking always exceeds the rise due to grain refinement [11].

Interestingly, compared with previous research done by Krishnaiah et al. [8], the processing efficiency in our work is higher. For grain refinement, subgrains of about 0.5 μm with a lower dislocation density inside are obtained, instead of dislocation cells. OM observations show a mean grain size of around 21 μm with a more homogeneous distribution at the last pass. Correspondingly, tensile properties have experienced a large and rapid change from the initially low strengths and high elongation. Actually, the subgrains have already appeared at Pass 1 and the effective property improvement nearly saturates during this stage. Peng et al. have proposed a "bend-affected zone" in the pure shear region in their research [5]. The zone is induced by the extension of deformation around the groove corner. In this study, a smaller groove width of 2 mm and full constraint from the dies can enhance the effect of interface regions on the deformation of adjacent shear regions. This effect can be alleviated by the free elongation along the longitudinal direction of samples under the conditions of (unconstrained) groove pressing. Thus, we conclude that the processing rate is determined not only by the pass number but also by the die structure, such as groove width and constraint. In other words, die condition will influence the effective strain amount accumulated in the sample. For example, a small groove width and tight constraint indeed enhance the strain accumulation. However, due to more severe plastic deformation induced under this condition, initiation and propagation of micro-cracks occur much earlier, and consequently, the effective pass number is limited.

4.3. Electrical resistivity

In this research, the influence of SPD by CGP on the evolution of electrical resistivity of pure copper sheets has been investigated for the first time. The variation of electrical resistivity against pass number is presented in **Figure 6**. As can be seen, the annealed copper has an initial electrical resistivity of about 1.87 μΩ·cm, and it is positively correlated to the effective strain. The most rapid increase appears at the first pass. A decrease of the slope of variation curve is observed during the subsequent passes. The value of the electrical resistivity gets to the maximum of about 2.02 μΩ·cm after the third pass.

Crystalline defects such as impurities, dislocations and grain boundaries contribute to the resistivity of copper. SPD usually leads to the changes of grain size and dislocation density in

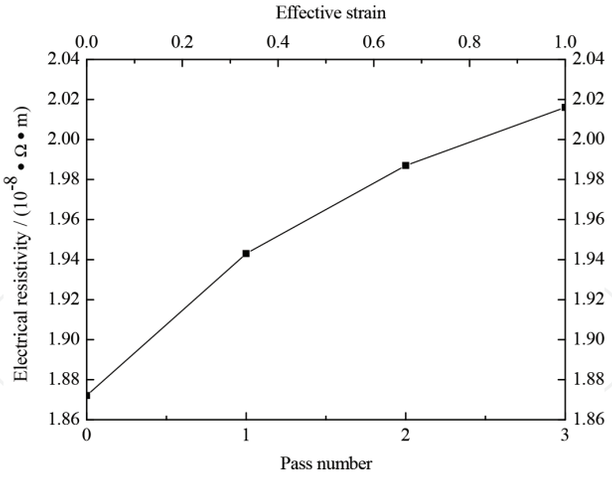

Figure 6. Variation of electrical resistivity against pass number.

metallic materials. As for pure metal, the microstructural effect on the electrical resistivity mainly comes from imperfections such as grain boundary and dislocation. Both of them play important roles in electron scattering, which will increase the electrical resistivity significantly [12].

During CGP, the microstructure of the material is characterized by noticeable grain refinement and high dislocation density. Refining the microstructure causes the increase of the total surface. Consequently, the electrical resistivity increases rapidly at the initial stages. Meanwhile, the occurrence of micro-cracks also contributes to the resistivity increase.

At a high level of plastic strain, there is a competition among dislocation recovery, homogeneity improvement and microcracking in deciding the electrical resistivity of materials. On one hand, recovery and rearrangement of dislocations happen at a larger magnitude of plastic strain, as indicated in **Figure 5b**, and slow down the dislocation proliferation and grain size reduction. Meanwhile, the improvement of microstructure distribution discussed above also helps to reduce the resistivity by homogenizing the various defects. On the other hand, micro-cracks nucleate and propagate on the sample surface, and the air gaps act as obstacles for electrons transport or scattering, resulting in the increase of electrical resistivity. Finally, a slightly lower increase rate of electrical resistivity is evident at Passes 2 and 3.

5. Influences of die structure on constrained groove pressing of commercially pure Ni sheets

5.1. Materials preparation and CGP experiments

Commercially pure Ni sheets with dimensions of 100 × 66 × 2 mm^3 were used. Before pressing, the cold-rolled sheets were fully annealed at 750°C for 4 h in an SX2-4-10 resistance-heated furnace utilizing high pure nitrogen as the protective atmosphere to ensure the annealing process. The mean grain size estimated by line intercept method is approximately 28 μm.

Table 5 gives the schemes of experiments in this work. Qualitatively, considering the sample thickness of 2 mm, a lower groove width may induce severe shear in the sheets, and inefficiency is expected with a lower angle. Meanwhile, either a higher width or angle may change the deformation characteristics of CGP. In order to improve the research efficiency, representative schemes were conducted, as shown in **Table 5**. The groove dies used in the laboratory are shown in **Figure 7**. When pressing, the groove direction was perpendicular to the rolling direction (RD) of the sheets, and Teflon layers were used as a lubricant.

5.2. Influences of die structure on mechanical properties

In the experiments, CGP process was repeated until distinct cracks appeared on the surface of sheet samples. **Figure 8** gives the tensile properties of the sheets in different schemes. Obviously, the number of effective passes varies with die structure, and it is five, four and three in Schemes 1, 2 and 3, respectively. Thus, compared with previous works carried out by Satheesh Kumar and Raghu [13, 14], the pass number in this study is increased by the reduction of either groove angle or friction coefficient (by using Teflon layers as a lubricant). However, it should be noted that, according to Eq. (3), in Scheme 1 only a total effective strain of about 0.87 is imposed to the samples per pass.

In all the three schemes, CGP indeed greatly improves the strength of pure Ni sheets. The initially annealed pure Ni sheets have a yield strength of 79.6 MPa and ultimate tensile strength of 398.1 MPa. In Scheme 1, the yield strength rapidly increases to 407.9 MPa after Pass 1 and reaches the peak value of 439.7 MPa at Pass 3 with a strain of 2.61. Then, it experiences a slight fall to 406.9 MPa during the following two passes. In Scheme 2, the maximum yield

Die structure	$\theta = 30^\circ$	$\theta = 37^\circ$	$\theta = 45^\circ$	$\theta = 53^\circ$	$\theta = 60^\circ$
$T = 1$ mm	–	–	S	–	–
$T = 2$ mm	S	S/E_1	S/E_2	S	S
$T = 3$ mm	–	–	S/E_3	–	–
$T = 4$ mm	–	–	S	–	–

Note: θ and T are groove angle and width, respectively. S represents numerical simulation; E_1, E_2 and E_3 represent Schemes 1, 2 and 3 in experiments, respectively.

Table 5. Schemes of experiments and numerical simulations.

(a) Scheme One (b) Scheme Two (c) Scheme Three

Figure 7. Groove dies used in the experiments. (a) Scheme 1; (b) Scheme 2; (c) Scheme 3.

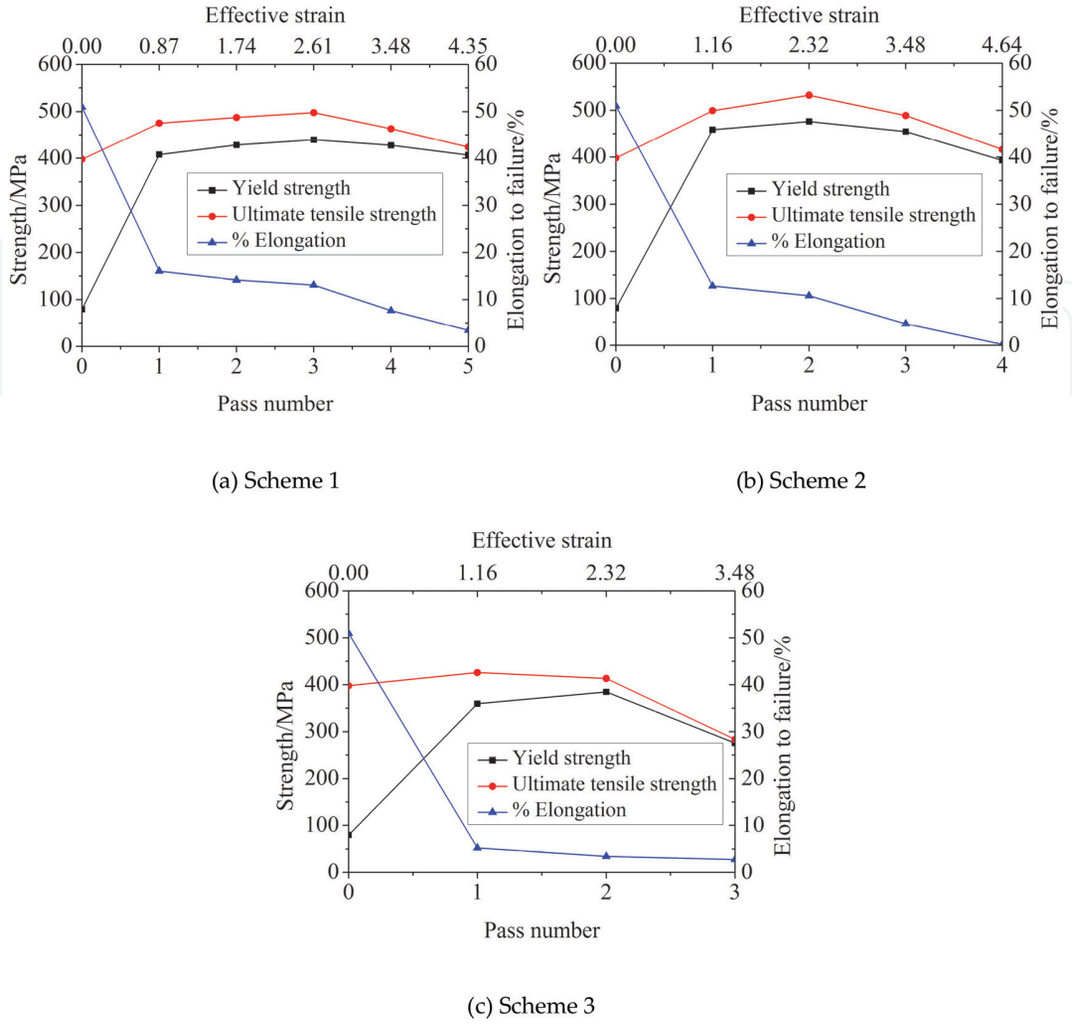

Figure 8. Tensile properties of Ni sheets before and after CGP. (a) Scheme 1; (b) Scheme 2; (c) Scheme 3.

strength of 476.3 MPa appears at Pass 2. After that, a decrease is observed, too. However, the highest strength is only 384.7 MPa at Pass 3 in Scheme 3. Meanwhile, it is observed that the evolution of tensile strength with pass number shows a similar trend to that of yield strength, but the increase of tensile strength at Pass 1 is not so significant, especially in Scheme 3. In addition, the elongation to failure of the annealed pure Ni sheets is about 51.0%, and all CGP samples experience a remarkable decrease at Pass 1. From Schemes 1–3, there is a gradual reduction in elongation of the processed materials, indicating a decrease of ductility caused by the increase of either groove width or angle [15].

The grain refinement and work hardening lead to the strength increase of materials during the initial stage of CGP, while the mechanisms of micro-cracking and flow softening contribute to the decrease at the later passes [10]. In this work, the optimum tensile properties of CGP pure Ni are obtained by the die design in Scheme 2. In Scheme 1, a lower groove angle relieves the intensity of shear deformation and also brings about more effective passes. Besides, the sheets processed in this scheme have a more acceptable ductility, but lower levels of total strain and strength than those in Scheme 2. Importantly, in Scheme 3, a larger groove width does not

allow more CGP passes. Actually, materials get the worst results of property improvement in this scheme.

Figure 9 presents the evolution of average microhardness with pass number in different schemes. Generally, for all schemes, a sharp increase is observed from an initial value of 90.0 HV, and after that, only a slight increase is obtained. No reduction in hardness happens due to flow softening, indicating that micro-cracking plays a more important role than flow softening in the decrease of strength. Different from strength, the average hardness of CGP materials in Scheme 3 is higher than that in Scheme 1 during the three effective passes. However, at Pass 5 in Scheme 1, the final hardness catches up with that at Pass 3 in Scheme 3. This suggests the importance of strain amount in the enhancement of mechanical properties. In addition, despite the same rate of strain accumulation in Schemes 2 and 3, a higher level of hardness is observed in Scheme 2. Thus, it is believed that, besides strain amount, there must be other factors based on the change of die structure accounting for this result. And this will be discussed in the following sections.

Briefly in this work, with a groove width of 2 mm and a groove angle of 45° in Scheme 2, pure Ni sheets with a thickness of 2 mm processed by a two-pass CGP acquire the best mechanical properties. The yield and tensile strengths are 476.3 and 532.3 MPa, respectively, the elongation to failure is 10.6%, and the average microhardness is 218.9 HV.

5.3. Influences of die structure on microstructure

Figure 10 shows the TEM micrographs and corresponding SAED patterns of CGP pure Ni sheets at the last pass in different experimental schemes. In **Figure 10a**, only irregular dislocation cells can be found in the microstructure even processed with a total strain of 4.35. The cell structures with high dislocation density both inside and at the boundaries are not homogeneous. Similar substructures appear in Scheme 3, as illustrated in **Figure 10c**. However, the less diffused SAED pattern indicates lower misorientation angles between cells in Scheme 3 due to a smaller strain amount of 3.48.

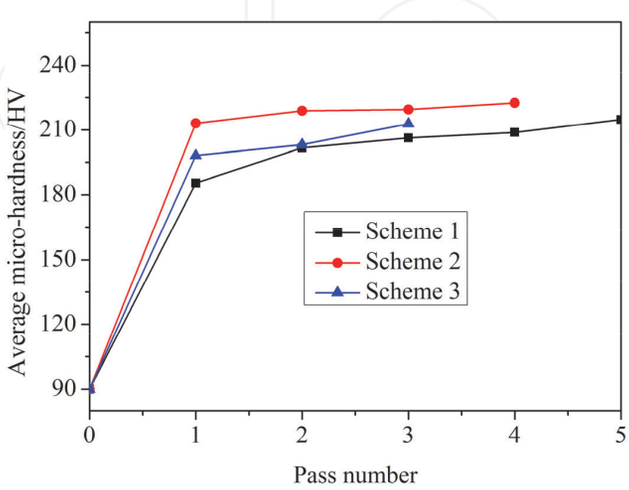

Figure 9. Average micro-hardness of Ni sheets before and after CGP.

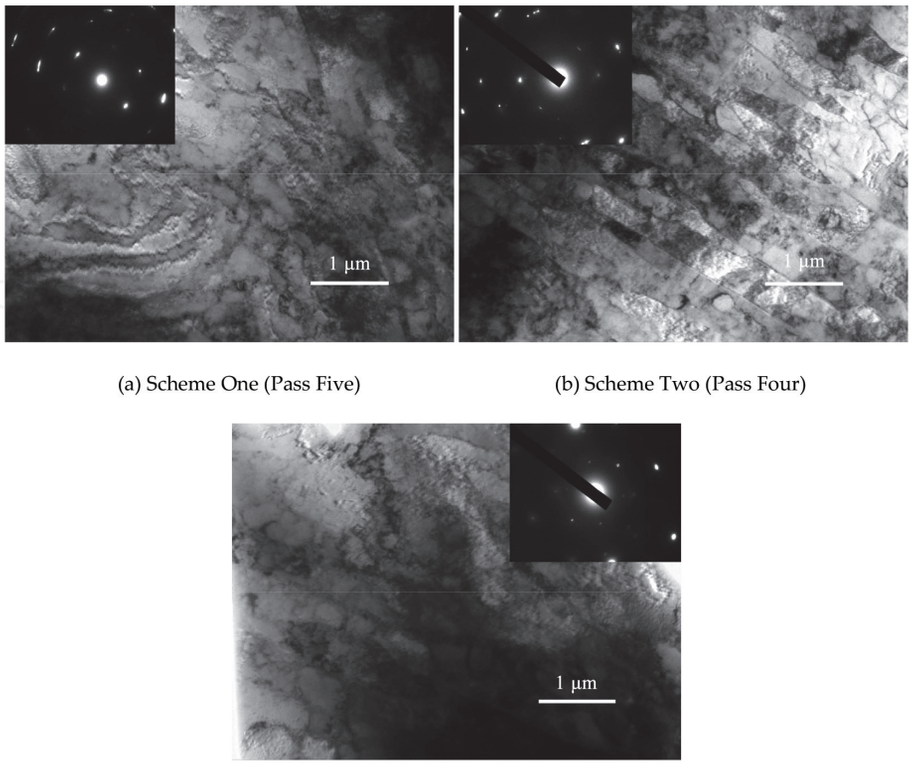

(a) Scheme One (Pass Five) (b) Scheme Two (Pass Four)

(c) Scheme Three (Pass Three)

Figure 10. TEM micrographs and corresponding SAED patterns of CGP Ni sheets. (a) Scheme 1 (Pass 5); (b) Scheme 2 (Pass 4); and (c) Scheme 3 (Pass 3).

Corresponding to the optimum mechanical properties, the die design in Scheme 2 leads to the best results of grain refinement. As shown in **Figure 10b**, a large number of elongated subgrains come into being with a mean width of about 500 nm. Separate grains with clear boundaries and high misorientation angles indicated by the SAED pattern are obtained. Compared with pure Cu [11], the material in this work experiences a higher efficiency of grain refinement due to its intermediate SFE.

5.4. Influences of die structure on texture evolution

Small crystalline size and lattice distortion are two principal imperfections in crystalline materials and usually cause peak broadening in XRD patterns compared with those attained from perfect crystal diffraction. Thus, the evolutions of cell size and lattice micro-strain can be reflected by the deviation of line profile from perfect diffraction. In this work, XRD patterns of pure Ni sheets before and after one CGP pass in different experimental schemes were examined and presented in **Figure 11**. Clearly, diffractions from four crystalline planes are more intense than those from others, and they are (111), (200), (220) and (311). Considering the diffractions of these peaks on all samples, the microstructure evolution can be analyzed. Compared with the annealed pure Ni sheets, the peaks exhibit different degrees of broadening after Pass 1, suggesting various results of grain refinement. Specifically, the most and least distinct broadenings can be carefully observed in Schemes 2 and 3, respectively. This confirms the TEM observations of microstructure evolution discussed above.

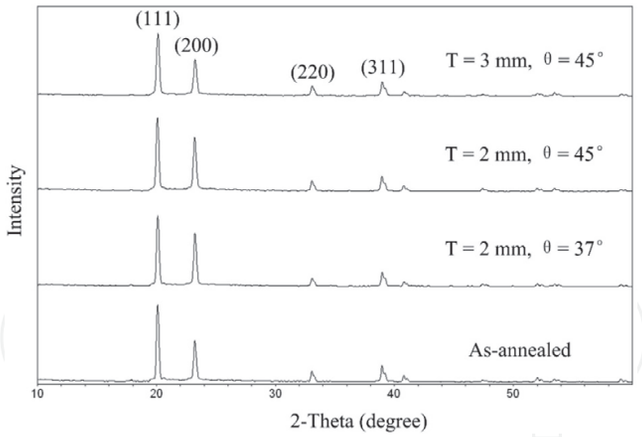

Figure 11. XRD patterns of Ni sheets before and after Pass 1.

6. Conclusions

1. The best parameter combination is A3B3C3D2 under the established conditions. The deformation is the most homogeneous when groove width is 2 mm, groove angle is 60°, the friction coefficient is 0.12 and deformation rate is 1.6 mm/s. The I.F. value of optimum model drops by about 50% and the deformation homogeneity is greatly improved. Compared with the initial model, plastic strain accumulated in samples deformed by the same number of passes increases to almost twice. The deformation efficiency of CGP technique is promoted significantly.

2. A four-pass CGP was carried out on commercially pure aluminum sheets. The grain size is refined from 29 μm of the annealed sample to 18 μm after four passes. Dislocation-free subgrains of the submicron level with well-defined boundaries are obtained. The ultimate tensile strength and yield strength have been improved significantly. All the load-stroke curves can be divided into three stages: rapid increase, moderate increase and second rapid increase. During flattening, a short plateau appears at the beginning of the second stage.

3. For commercially pure copper sheets, the grain size is reduced from 30 μm of the annealed material to around 21 μm after CGP deformation, and subgrains sized about 0.5 μm with distinct boundaries are obtained at Pass 3. The sharp changes of microstructure and mechanical properties indicate a high processing efficiency of this technique with a small groove width of 2 mm and tight constraint. The electrical resistivity of pure copper exhibits a near-linear increase with the straining. Crystalline imperfections, microcracking and microstructure uniformity together determine the evolution of electrical resistivity.

4. For pure Ni sheets, the optimum mechanical properties of pure Ni sheets with a thickness of 2 mm are obtained by a groove width of 2 mm and a groove angle of 45° after two CGP passes. In the experiments, a lower groove angle eases the intensity of shear deformation and permits more effective passes while the process efficiency is reduced. Besides, a higher groove width cannot induce more passes but obtain the worst CGP results. In both

cases, only cell structures with high dislocation density are observed. The peak broadenings in XRD patterns of pure Ni sheets after CGP confirm the results of grain refinement indicated by TEM observations: Scheme 2 > Scheme 1 > Scheme 3.

Acknowledgements

The research work was supported by the National Natural Science Foundation of China (51375269, 51675307).

Author details

Yanjin Guan[1]* and Zongshen Wang[2]

*Address all correspondence to: guan_yanjin@sdu.edu.cn

1 Key Laboratory for Liquid-Solid Structural Evolution and Processing of Materials (Ministry of Education), Shandong University, Jinan, China

2 School of Mechanical Engineering, Shandong University of Technology, Zibo, China

References

[1] Shin DH, Park J, Kim Y, Park K. Constrained groove pressing and its application to grain refinement of aluminum. Materials Science and Engineering: A. 2002;**328**:98-103

[2] Shirdel A, Khajeh A, Moshksar MM. Experimental and finite element investigation of semi-constrained groove pressing process. Materials & Design. 2010;**31**:946-950

[3] Borhani M, Djavanroodi F. Rubber pad-constrained groove pressing process: Experimental and finite element investigation. Materials Science and Engineering: A. 2012;**546**:1-7

[4] Sajadi A, Ebrahimi M, Djavanroodi F. Experimental and numerical investigation of Al properties fabricated by CGP process. Materials Science and Engineering: A. 2012;**552**:97-103

[5] Peng K, Zhang Y, Shaw LL., Qian KW. Microstructure dependence of a Cu-38Zn alloy on processing conditions of constrained groove pressing. Acta Materialia. 2009;**57**:5543-5553

[6] Peng K, Su L, Shaw LL, Qian KW. Grain refinement and crack prevention in constrained groove pressing of two-phase Cu-Zn alloys. Scripta Materialia. 2007;**56**:987-990

[7] Wang ZS, Liang P, Guan YJ, Liu YX, Jiang LB. Experimental investigation of pure aluminum sheets processed by constrained groove pressing. Indian Journal of Engineering and Materials Sciences. 2014;**21**:121-127

[8] Krishnaiah A, Chakkingal U, Venugopal P. Applicability of the groove pressing technique for grain refinement in commercial purity copper. Materials Science and Engineering: A. 2005;**s410–s411**:337-340

[9] Khodabakhshi F, Kazeminezhad M, Kokabi AH. Constrained groove pressing of low carbon steel: Nano-structure and mechanical properties. Materials Science and Engineering: A. 2010;**527**:4043-4049

[10] Hosseini E, Kazeminezhad M. Nanostructure and mechanical properties of 0-7 strained aluminum by CGP: XRD, TEM and tensile test. Materials Science and Engineering: A. 2009;**526**:219-224

[11] Wang Z.S, Guan YJ, Liang P. Deformation efficiency, homogeneity, and electrical resistivity of pure copper processed by constrained groove pressing. Rare Metals. 2014;**33**:287-292

[12] Khodabakhshi F, Kazeminezhad M. The effect of constrained groove pressing on grain size, dislocation density and electrical resistivity of low carbon steel. Materials & Design. 2011;**32**:3280-3286

[13] Satheesh Kumar SS, Raghu T. Tensile behaviour and strain hardening characteristics of constrained groove pressed nickel sheets. Materials & Design. 2011;**32**:4650-4657

[14] Satheesh Kumar SS, Raghu T. Mechanical behaviour and microstructural evolution of constrained groove pressed nickel sheets. Journal of Materials Processing Technology. 2013;**213**:214-220

[15] Wang ZS, Guan YJ, Wang GC, Zhong CK. Influences of die structure on constrained groove pressing of commercially pure Ni sheets. Journal of Materials Processing Technology. 2015;**215**:205-218